Substrate-Triggered Activation of a Synthetic [Fe$_2$(μ-O)$_2$] Diamond Core for C−H Bond Cleavage

Genqiang Xue, Alexander Pokutsa,[†] and Lawrence Que, Jr.*

Department of Chemistry and Center for Metals in Biocatalysis, University of Minnesota, Minneapolis, Minnesota 55455, United States

S *Supporting Information*

ABSTRACT: An $[Fe^{IV}_2(\mu\text{-O})_2]$ diamond core structure has been postulated for intermediate **Q** of soluble methane monooxygenase (sMMO-**Q**), the oxidant responsible for cleaving the strong C−H bond of methane and its hydroxylation. By extension, analogous species may be involved in the mechanisms of related diiron hydroxylases and desaturases. Because of the paucity of well-defined synthetic examples, there are few, if any, mechanistic studies on the oxidation of hydrocarbon substrates by complexes with high-valent $[Fe_2(\mu\text{-O})_2]$ cores. We report here that water or alcohol substrates can activate synthetic $[Fe^{III}Fe^{IV}(\mu\text{-O})_2]$ complexes supported by tetradentate tris(pyridyl-2-methyl)amine ligands (**1** and **2**) by several orders of magnitude for C−H bond oxidation. On the basis of detailed kinetic studies, it is postulated that the activation results from Lewis base attack on the $[Fe^{III}Fe^{IV}(\mu\text{-O})_2]$ core, resulting in the formation of a more reactive species with a $[X\text{−Fe}^{III}\text{−O−Fe}^{IV}\text{=O}]$ ring-opened structure (**1−X**, **2−X**, X = OH$^-$ or OR$^-$). Treatment of **2** with methoxide at −80 °C forms the **2**−methoxide adduct in high yield, which is characterized by an $S = 1/2$ EPR signal indicative of an antiferromagnetically coupled $[S = 5/2\, Fe^{III}/S = 2\, Fe^{IV}]$ pair. Even at this low temperature, the complex undergoes facile intramolecular C−H bond cleavage to generate formaldehyde, showing that the terminal high-spin Fe^{IV}=O unit is capable of oxidizing a C−H bond as strong as 96 kcal mol^{-1}. This intramolecular oxidation of the methoxide ligand can in fact be competitive with intermolecular oxidation of triphenylmethane, which has a much weaker C−H bond ($D_{C−H}$ 81 kcal mol^{-1}). The activation of the $[Fe^{III}Fe^{IV}(\mu\text{-O})_2]$ core is dramatically illustrated by the oxidation of 9,10-dihydroanthracene by **2**−methoxide, which has a second-order rate constant that is 3.6×10^7-fold larger than that for the parent diamond core complex **2**. These observations provide strong support for the DFT-based notion that an $S = 2$ Fe^{IV}=O unit is much more reactive at H-atom abstraction than its $S = 1$ counterpart and suggest that core isomerization could be a viable strategy for the $[Fe^{IV}_2(\mu\text{-O})_2]$ diamond core of sMMO-**Q** to selectively attack the strong C−H bond of methane in the presence of weaker C−H bonds of amino acid residues that define the diiron active site pocket.
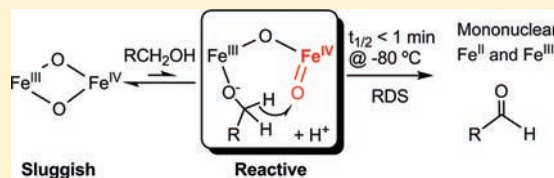
INTRODUCTION

Nonheme diiron enzymes catalyze the oxidation of various substrates by the activation of dioxygen. This class includes soluble methane monooxygenase (sMMO), related bacterial multicomponent monooxygenases, and fatty acid desaturases.[1−6] High-valent intermediates are implicated in the oxygen activation mechanisms for these enzymes.[3,5−7] For example, intermediate **Q** of sMMO is a two-electron oxidant that effects the hydroxylation of methane[8−14] and has been proposed to have an $[Fe^{IV}_2(\mu\text{-O})_2]$ diamond core on the basis of extended X-ray absorption fine structure (EXAFS) studies.[15] Related diiron(IV) oxidants may also be involved in the catalytic cycles of fatty acid desaturases and other diiron monooxygenases resulting from cleavage of the O−O bond in observed peroxo intermediates,[16−18] but direct evidence for such diiron(IV) species has not yet been obtained. Similar oxygen activation chemistry is utilized by ribonucleotide reductases (RNR) with diiron and iron−manganese centers, which generate a one-electron oxidant called **X** that is needed to oxidize a specific Cys residue that initiates the deoxygenation of ribonucleotides to deoxyribonucleotides.[19] For these enzymes, Fe^{III}M^{IV} (M = Fe or Mn) oxidants have been trapped and characterized,[20,21] and the intermediate for the RNR from *Chlamydia tranchomatis* has been proposed to have an $[Fe^{III}\text{-}Mn^{IV}(\mu\text{-O})(\mu\text{-OH})]$ diamond core on the basis of Fe and Mn K-edge EXAFS experiments and associated density functional theory (DFT) calculations.[22]

The hydroxylation of a variety of alkanes by sMMO-**Q** exhibits an interesting reactivity pattern via a mechanism that is not yet fully understood. For example, the reactions of **Q** with methane and ethane give rise to nearly identical second-order rate constants,[12,23] despite the fact that the former has a 4.5 kcal mol^{-1} higher bond dissociation energy ($D_{C−H}$ = 105 kcal mol^{-1} versus 100.5 kcal mol^{-1}).[24] Moreover, large deuterium kinetic isotope effect (KIE) values in the range of 23−42 were found in the oxidation of methane by **Q**, but no KIE was detected for ethane oxidation.[11,12,23] These results were rationalized by a proposed two-step mechanism where substrate binds to form a **Q·S** adduct that then undergoes C−H bond cleavage.[11,12,23,25] Access to **Q** is governed by the size of the substrate,[12,26,27] and

Scheme 1. Core Structures and Supporting Ligands of Complexes 1−4
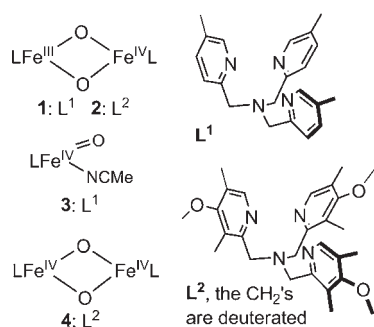
Scheme 2. Reactions of the $[Fe^{III}Fe^{IV}(\mu\text{-}O)_2]$ Diamond Core with Hydroxide[37] or Alkoxides
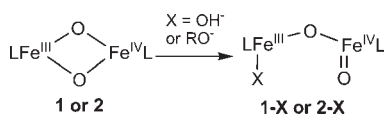
only methane is small enough to be able to bind rapidly and make C−H bond cleavage the rate-determining step.[12,23,25]

On the other hand, the extremely high reactivity associated with **Q** might cause oxidation of weaker C_α−H bonds on the protein backbone.[28,29] The fact that such side reactions do not readily occur during catalytic turnover suggests that the enzyme must employ some strategies to minimize protein self-oxidation. It is thus plausible that substrate binding may be used as a trigger to unmask a more reactive oxidant that carries out the difficult C−H bond cleavage step on the substrate oxidation pathway. Indeed, some DFT calculations have raised the possibility that $[Fe^{III}\text{−}O\text{−}Fe^{V}\text{=}O]$ (by Siegbahn and Crabtree)[30] or $[Fe^{III}(\mu\text{-}O)_2Fe^{V}]$ (by Friesner and co-workers)[31] isomers of the $[Fe^{IV}_2(\mu\text{-}O)_2]$ diamond core may be involved in methane oxidation, although experimental evidence for such an intermediate has yet to been obtained.

This notion of core isomerization for **Q** to generate a more reactive oxidant has also developed from reactivity studies of synthetic diiron complexes. In the work of Caradonna and Rybak-Akimova on a diiron(II) catalyst for efficient hydroxylation of cyclohexane with ROOH as oxidant,[32] spectroscopic evidence has been found for the putative oxidant in the catalytic reaction, proposed to be an $[Fe^{II}Fe^{IV}\text{=}O]$ species, which in the absence of substrate isomerizes to the more stable $[Fe^{III}\text{−}O\text{−}Fe^{III}]$ product.[33,34] In our own work, we have characterized the first examples of complexes with $[Fe^{III}Fe^{IV}(\mu\text{-}O)_2]$ (**1** in Scheme 1)[35] and $[Fe^{IV}_2(\mu\text{-}O)_2]$ (**4** in Scheme 1)[36] core structures, providing synthetic precedents for the $[Fe^{IV}_2(\mu\text{-}O)_2]$ core proposed for **Q**.[15] However, these model complexes exhibit C−H bond oxidation reactivities that are 2−3 orders of magnitude lower than that of a closely related mononuclear oxoiron(IV) complex (**3** in Scheme 1).[36] This comparison suggests that bridging oxos in high-valent complexes may not be as reactive as terminal oxos in cleaving C−H bonds and raises an interesting question as to precisely what mechanisms may be involved in C−H bond oxidations by high-valent enzymatic and synthetic intermediates with the $[Fe_2(\mu\text{-}O)_2]$ diamond core. More recently, we reported that addition of hydroxide to complex **2** generates an open-core
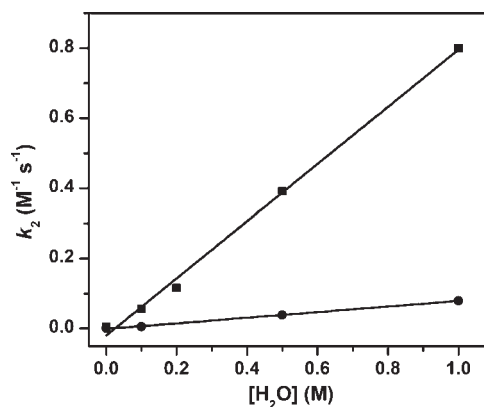

Figure 1. The second-order rate constants for oxidation of DHA (■) and DHA-d_4 (●) by **1** in MeCN −30 °C under Ar with different concentrations of added H_2O. The KIEs obtained at 0, 0.1, 0.5, and 1.0 M added H_2O are 9, 9, 10, and 10, respectively.

structure **2**−OH (Scheme 2), which oxidizes C−H bonds over a million-fold faster than **2** itself. Comparisons among a series of complexes with the same supporting tetradentate ligand revealed that this reactivity enhancement derives mainly from two principal factors: (1) the opening up of the $[Fe_2(\mu\text{-}O)_2]$ diamond core to form a terminal oxoiron(IV) moiety, and (2) the conversion of the $Fe^{IV}\text{=}O$ unit from $S = 1$ to $S = 2$.[37]

In this Article, we report that water and alcohols can also activate the diamond core of **1** and **2** for C−H bond oxidation. The mode of activation involves ROH coordination to the diamond core, resulting in the formation of a ring-opened hydroxo or alkoxo adduct (Scheme 2). In the latter case, coordination of an alkoxide generates an observable oxidant−substrate adduct, which can undergo intramolecular oxidation to generate the corresponding aldehyde (or ketone) product. With such adducts, the diamond core complexes can selectively oxidize the C−H bonds on alcohol substrates over nonbinding substrates, even when the latter have significantly weaker C−H bonds. This serves as an example of substrate activation on the $[Fe_2(\mu\text{-}O)_2]$ diamond cores, an activation mechanism that may be employed by enzymatic intermediates for selective substrate oxidation.

■ RESULTS AND DISCUSSION

C−H Bond Oxidation by Dinuclear Diamond Core Complexes. We have reported that the oxidation of 9,10-dihydroanthracene (DHA) by complex **1** at −30 °C in MeCN was enhanced by addition of H_2O and the enhancement exhibited a linear dependence on the concentration of added H_2O.[38] The second-order rate constant (k_2) in the presence of 1 M H_2O was found to be 200-fold higher than that in the absence of added H_2O.[38] These observations suggest the possibility that addition of H_2O converts **1** into a different species that acts as a more powerful oxidant. To test this hypothesis, we have investigated the kinetics of the oxidation of the deuterated substrate 9,9,10,10-d_4-DHA (DHA-d_4) for comparison with the results for the undeuterated substrate. Under all added H_2O concentrations studied, the oxidation rates for DHA-d_4 decrease significantly relative to those for DHA, indicating that H-atom abstraction is an important component of the rate-determining step. However, the measured H/D kinetic isotope effect (KIE) is
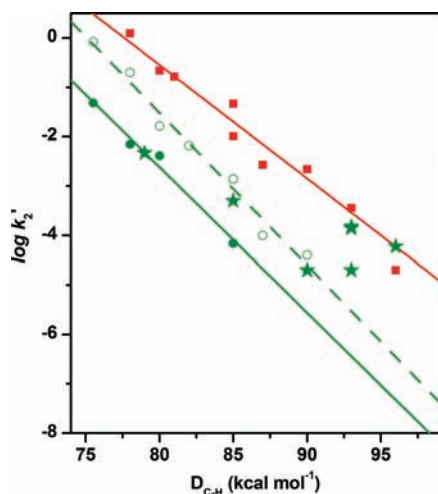
Figure 2. The log k_2' versus D_{C-H} plots for reactions of **3** with all substrates (■), **1** with hydrocarbon substrates (●) or with alcohol substrates (★) in the presence of 50 mM H_2O, and **1** with hydrocarbon substrates (○) in the presence of 1.0 M H_2O. The straight line for **3** was obtained by using the k_2' values of all substrates, while that for **1** was obtained by fitting only the k_2' values of hydrocarbon substrates. The k_2' values used for the plots and the reaction conditions are listed in Table S1.

Table 1. Product Yields for Substrate Oxidations by 1 and 2

oxidant	substrate	product/yield, %[a]	n−e⁻ oxidation to form product
1	xanthene	xanthone/25	4
1	DHA	anthracene/40	2
1	fluorene	fluorenone/23	4
1	benzyl alcohol	benzaldehyde/71	2
1	methanol	formaldehyde/83	2
2	DHA	anthracene/52	2
2	benzyl alcohol	benzaldehyde/80	2
2	1-hexanol	hexanal/80	2
2	methanol	formaldehyde/90	2

[a] All reactions were performed in MeCN at −30 °C under Ar. The product yields are indicated with respect to the concentration of the iron complex.

independent of H_2O concentration with values of 9−10 (Figure 1). As KIEs are determined by reaction conditions such as temperature, substrate, and properties of the oxidants,[39] the observation of the same KIE under all conditions strongly suggests that only one oxidant carries out the C−H bond cleavage step at all H_2O concentrations and that unactivated **1** by itself is quite a sluggish oxidant.

In the absence of any H_2O added to the MeCN solution,[40] only substrates with C−H bonds weaker than 80 kcal mol⁻¹, such as DHA (78 kcal mol⁻¹) and xanthene (75.5 kcal mol⁻¹) (see Table S1 for a list of D_{C-H} values for all substrates used in this study), are observed to be oxidized at rates fast enough to be distinguished from the self-decay of **1**. However, in the presence of 0.05 M H_2O, hydrocarbon substrates with D_{C-H} values of up to 85 kcal mol⁻¹ (tetralin) can be oxidized. As shown in Figure 2, the logarithms of the second-order rate constants normalized on a per active hydrogen (e.g., 4 for DHA and tetralin and 2 for
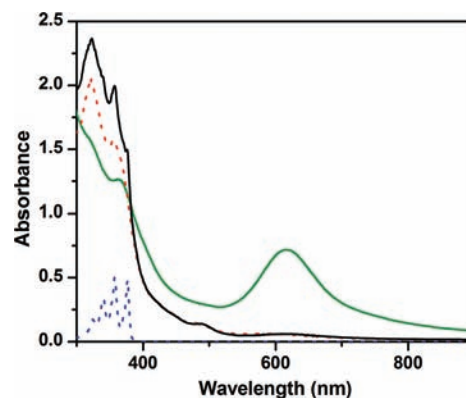

Figure 3. The UV−vis spectra of 0.15 mM complex **1** in MeCN (with 1 M H_2O) at −30 °C (green solid line) and the solution after reaction with 10 mM DHA (black solid line). The latter spectrum exhibits the absorption features of (a) a (μ-oxo)diiron(III) decay product (λ_{max} at 320, 350, and 490 nm) and (b) anthracene (λ_{max} at 357 and 377 nm). For comparison, spectra for corresponding authentic compounds (Fe^{III}−O−Fe^{III} and anthracene) in MeCN (with 1 M H_2O) at −30 °C are also shown, respectively, in red and blue dotted lines. See Figure S1 for time-resolved spectral changes and the time trace at 620 nm together with its fit to a first-order kinetic model.

fluorene) basis (k_2') show an inverse linear correlation with D_{C-H}. Similar inverse linear correlations have been observed in C−H bond oxidations by several mononuclear nonheme oxoiron(IV) complexes[41−44] and an iron(III)-methoxide complex,[45] consistent with a mechanism that involves rate-determining H-atom abstraction. The reactivity of complex **1** is further enhanced at 1 M added H_2O, and the oxidation of hydrocarbon substrates with D_{C-H} values of up to 90 kcal mol⁻¹ (toluene) can be measured. The log k_2' versus D_{C-H} plots in the presence of 0.05 and 1 M H_2O are essentially parallel with respective slopes of −0.29(3) and −0.31(2), suggesting that the same oxidant is involved under these two conditions.

Complex **1** oxidizes DHA in the presence of 1 M H_2O to anthracene (Table 1), as indicated by the appearance of its characteristic UV−vis features (λ_{max} at 377 and 357 nm) in the resulting solution (Figure 3). The observed 40% yield of anthracene suggests that 2 equiv of **1** is required to carry out the 2-e⁻ oxidation of DHA. This notion is corroborated by the appearance of UV−vis features of an oxo-bridged diiron(III) product (λ_{max} at 320, 350, and 490 nm)[35] in the product solution (Figure 3) and the observation that the latter is EPR silent. A similar diiron(III) product is observed for the oxidation of xanthene and fluorene by **1**. The latter are respectively converted to 4-e⁻ oxidized derivatives, xanthone and fluorenone, in about 25% yield (Table 1). Taken together, these results demonstrate that **1** acts effectively as a 1-e⁻ oxidant in the oxidation of these hydrocarbon substrates.

C−H Bond Oxidation by Mononuclear Oxoiron(IV) Complex 3. The $S = 1$ oxoiron(IV) complex **3**[46] can oxidize a similar series of substrates at −30 °C, but with D_{C-H} values ranging from 78 to 96 kcal mol⁻¹. The normalized second-order rate constants are listed in Table S1 and plotted in Figure 2 versus corresponding D_{C-H} values. Interestingly, the oxidation rates associated with **3** are approximately 2 orders of magnitude higher than those of **1** in the presence of 50 mM H_2O. Second, the DHA oxidation rate of **3** is unaffected by the presence of 1 M H_2O showing that, unlike **1**, **3** is not activated by H_2O. Third, the log k_2' versus
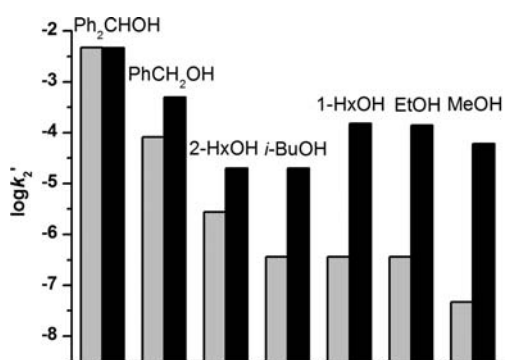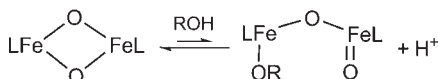
Figure 4. The projected (gray columns) and measured (black columns) log k_2' for oxidation of alcohols by **1** in MeCN with 50 mM H_2O. Conditions: -30 °C under Ar. The alcohols used as substrates from left to right are diphenylmethanol, benzyl alcohol, 2-hexanol, isobutanol, hexanol, ethanol, and methanol.

Scheme 3. Proposed Binding Equilibrium of Alcohol to the $[Fe_2(\mu\text{-}O)_2]$ Diamond Core

D_{C-H} plot (Figure 2) has a slope of $-0.22(1)$, which is comparable to those measured in oxidations by two other $S = 1$ oxoiron(IV) complexes $[Fe^{IV}(O)(N4Py)]^{2+}$ (-0.18) and $[Fe^{IV}\text{-}(O)(Bn\text{-}tpen)]^{2+}$ (-0.19) (N4Py = N,N-bis(2-pyridylmethyl)-bis(2-pyridyl)methylamine; Bn-tpen = N-benzyl-N,N',N'-tris(2-pyridylmethyl)-1,2-diaminoethane),[41] but notably smaller than the slopes for oxidation by **1** with 50 mM or 1 M added H_2O (-0.29 and -0.32, respectively). The steeper slopes for the log k_2' versus D_{C-H} correlation of **1**+H_2O suggest the involvement of an oxidant that differs in nature from the thus far characterized $S = 1$ oxoiron(IV) complexes.

Alcohol Oxidation by Diamond Core Complexes. While the oxidation rates of alcohol substrates by **3** fall on the line defined by the hydrocarbon substrates in the log k_2' versus D_{C-H} plot, the corresponding rates for oxidation by **1** generally deviate from the corresponding line for **1** (Figure 2, also see Figure S2 for an example of time-resolved spectral changes during methanol oxidation as well as the time trace at 616 nm together with its fit to a first-order kinetic model). The oxidation of methanol by **1** in MeCN with 50 mM H_2O has a rate that is over 3 orders of magnitude higher than the extrapolated rate from the log k_2' versus D_{C-H} plot for hydrocarbon oxidation under the same conditions. Indeed, the oxidation of methanol by **1** is even faster than that by **3**. On the other hand, primary alcohols exhibit smaller rate enhancements, which inversely depend on the size of the alkyl substituents. For example, ethanol and 1-hexanol oxidation rates are larger by almost 3 orders of magnitude, while benzyl alcohol and isobutanol rates are less than 10-fold above values predicted by the log k_2' versus D_{C-H} plot. In addition, the oxidation rates for primary alcohols are enhanced more than secondary alcohols relative to their predicted values based on D_{C-H} values. For example, the rate for 1-hexanol is $\sim$6-fold greater than that for 2-hexanol, although the latter substrate has a smaller D_{C-H} and a higher projected rate. Notably, the secondary alcohol diphenylmethanol exhibits no rate enhancement at all. Thus, some additional factor besides D_{C-H} values is affecting
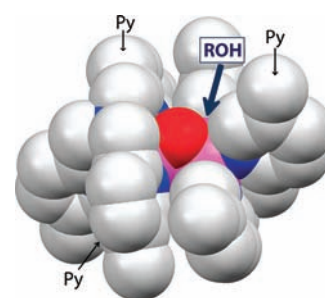

Figure 5. A space-filling model showing the $[Fe^{III}Fe^{IV}(\mu\text{-}O)_2]$ core structure of **1**. Note that the complexes are valence-delocalized complexes and centrosymmetric, so the two iron centers (pink atoms) are equivalent. The approach of the alcohol substrate (ROH) to an iron center is hindered by pyridine rings (Py) from the two tetradentate ligands.
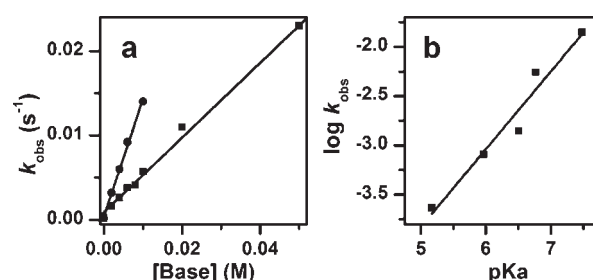

Figure 6. Effects of added bases on the oxidation rate of 1 M CH_3OH by **1** in dry MeCN at -30 °C under Ar. (a) Plot of k_{obs} versus [2,6-lutidine] (■) and [2,4,6-collidine] (●). (b) Plot of log k_{obs} versus pK_a in the presence of 10 mM added base. The pK_a's used are values for the conjugate acids of pyridine (5.17), 5-ethylpyridine (5.97), 2-methyl-5-ethylpyridine (6.51), 2,6-lutidine (6.77), and 2,4,6-collidine (7.48) in H_2O.[47] See Table S2 for a list of observed k_{obs} values.

the alcohol oxidation rates, which appears to correlate with the steric bulk of the alcohol. As illustrated by Figure 4, the smaller is the R group, the larger is the rate enhancement observed.

The apparent dependence of the rate enhancements on steric factors can be most easily rationalized by postulating the pre-equilibrium coordination of the alcohol substrate to one of the Fe atoms of **1** prior to substrate oxidation (Scheme 3). Binding of the alcohol would result in the opening of the $[Fe_2(\mu\text{-}O)_2]$ diamond core and generation of a terminal $Fe^{IV}=O$ moiety, analogous to what we have demonstrated in the reaction of **2** with OH^- (Scheme 2).[37] An examination of the structure of **1** shows that the $[Fe_2(\mu\text{-}O)_2]$ core can only be accessed via a $\sim$3-Å-wide slot defined by the pyridine rings of the two tetradentate ligands (Figure 5). The smaller is the alcohol, the more easily it can approach the $[Fe_2(\mu\text{-}O)_2]$ core and bind to one of the iron centers, resulting in the opening up of the core.

The existence of the above equilibrium was corroborated by the addition of bases, which would be expected to shift the equilibrium further to the right and enhance the rate of methanol oxidation. Indeed, as shown in Figure 6a, the first-order rate constant (k_{obs}) for the oxidation of 1 M CH_3OH increases linearly as a function of 2,6-lutidine or 2,4,6-collidine concentration, and 50 mM of 2,6-lutidine enhances the k_{obs} by a factor of 100 (Table S2). Moreover, there is also a linear correlation between the log k_{obs} values obtained upon addition of various bases and the pK_a's of the corresponding conjugate acids
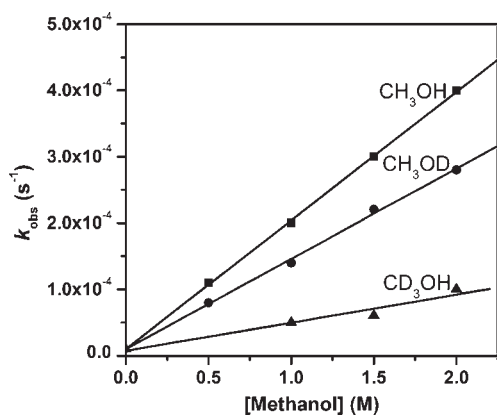
Figure 7. k_{obs} versus [substrate] plot for oxidation of CH_3OH, CH_3OD, and CD_3OH in dry MeCN at -30 °C. The KIEs are 1.4 and 4.5 for CH_3OD and CD_3OH, respectively.

(Figure 6b). Both plots strongly suggest that the equilibrium in Scheme 3 is shifted toward the formation of $1-OCH_3$ upon addition of base.

Interestingly, however, even in the presence of 1 M methanol and 10 mM 2,4,6-collidine, there was no obvious decrease in the amount of **1** that can be discerned by UV–vis spectroscopy, suggesting that the more reactive species represented at best a very minor fraction of the reaction mixture.[48] In principle, the concentration of this highly reactive species could be increased by raising the concentration of 2,4,6-collidine or using a stronger base, but the resulting solutions decayed very quickly at -30 °C, preventing its observation. As will be discussed in the next section, a somewhat more stable analogue of the proposed alkoxide adduct $1-OCH_3$ could be trapped at even lower temperature and spectroscopically characterized.

Kinetic isotope effect measurements provided further insight into the oxidation of methanol by **1**. As shown in Figure 7, methanol oxidation can be associated with two KIEs: 4.5 for deuteration of the methyl group and 1.4 for deuteration of the hydroxyl group. The observation of the C–H/D KIE suggests that H-atom abstraction from the methyl C–H bonds is an important component of the rate-determining step. On the other hand, we propose that the observed O–H/D KIE of 1.4 originates from pre-equilibrium binding of methanol to **1**, resulting in the formation of $1-OCH_3$ (Scheme 3). As CH_3OD would be expected to be less acidic than CH_3OH by about one pK_a unit, by analogy to the difference in the pK_a values for H_2O and D_2O,[49] the larger pK_a for CH_3OD would then result in a lower concentration of $1-OCH_3$ and consequently a slower oxidation rate observed for CH_3OD. Addition of 10 mM 2,6-lutidine gives rise to a similar O–H/D KIE of 1.6 (Figure S3), suggesting that the deprotonation step is indeed involved in the activation of methanol oxidation by added bases.

The binding equilibrium illustrated in Scheme 3 can also be used to rationalize the activation of **1** by the addition of H_2O. The active oxidant formed would then be the corresponding $1-OH$ species. (The analogous $2-OH$ species has been trapped by alternative approaches and spectroscopically characterized.[37]) This speculation is supported by the fact that replacing H_2O by D_2O resulted in a decrease in the rate of DHA oxidation by **1**. A kinetic solvent isotope effect value of 1.5 was obtained (Figure S4), which is similar to that observed for CH_3OH/CH_3OD. Moreover, addition of 2,6-lutidine to a solution of **1** in MeCN in

the presence of 1 M H_2O significantly enhanced the oxidation rate, as a linear function of the concentration of 2,6-lutidine (Figure S5).

CH_3OH appears to be less effective than H_2O for activation of the $[Fe_2(\mu\text{-}O)_2]$ diamond core, as suggested by the following observations: (1) addition of 1 M CD_3OD (used to minimize the contribution of bound-methoxide oxidation to the decay of **1**) to **1** enhances xanthene oxidation by less than 2-fold, while the enhancement by 1 M H_2O is over 100-fold; (2) it requires 50 mM 2,6-lutidine to enhance CH_3OH oxidation 100-fold (see Table S2), but only 4 mM 2,6-lutidine to obtain a 100-fold enhancement of the DHA oxidation rate by **1**+H_2O (Table S5). As compared to CH_3OH, H_2O has a smaller self-dissociation constant (14 versus 15)[49] and is sterically less bulky, so the equilibrium shown in Scheme 3 lies further to the right in the presence of H_2O.

Like **1**, **2** can also oxidize hydrocarbon and alcohol substrates under the same conditions (Table 1). However, the observed rates are slower due to the presence of additional electron-donating substituents on the pyridine rings of the supporting tetradentate ligand that stabilize the iron(IV) oxidation state.[36] For example, the rates for DHA and methanol oxidation by **1** are, respectively, 7- and 12-fold higher than those by **2** (Table S3). Moreover, the oxidatively susceptible benzylic C–H bonds of **2** are deuterated to hinder self-decay by ligand oxidation.[50] These two ligand design features make **2** a better choice for determining the product yields for substrates with stronger C–H bonds, such as the alcohol substrates in Table 1, and trapping the reactive oxidant–substrate adduct (see next section).

Besides exhibiting oxidation rates faster than expected from the green line in the plot shown in Figure 2, the reactions of **1** with alcohol substrates afford higher yields of oxidized product (Table 1). While the yields for oxidation of hydrocarbon substrates by **1** clearly show that it is acting as an 1-e$^-$ oxidant, the yields for methanol and benzyl alcohol oxidations are significantly higher than 50% (83% formaldehyde and 71% benzaldehyde, respectively) and suggest the involvement of a 2-e$^-$ process. As oxidation rates for alcohol substrates are typically slow due to their strong C–H bonds, ligand oxidation can compete with substrate oxidation and result in the underestimation of the product yields. Therefore, we used **2** to circumvent this problem. As shown in Table 1, **2** oxidizes alcohol substrates to afford aldehyde products in 80–90% yield, clearly showing that **1** and **2** act as 2-e$^-$ oxidants of alcohols.

An $Fe^{II}Fe^{III}$ product would thus be expected to form in the above alcohol oxidations. This notion was tested with **2**. The reaction solution at the end of the reaction of **2** and methanol was examined by EPR and NMR, which indicated that the expected diiron(II,III) product had disintegrated into mononuclear components. The EPR spectrum exhibited an isotropic signal at $g = 4.29$ associated with a high-spin mononuclear iron(III) byproduct having an intensity that corresponds 120% of the original concentration of **2**. The NMR spectrum of an analogous solution obtained in CD_3CN exhibited signals identical to that measured from the independently synthesized low-spin Fe(II) complex (δ (ppm, in CD_3CN) 9.12 (3H, br, α-pyr), 3.39 (9H, OCH_3), 1.84 (9H, CH_3), 1.74 (9H, CH_3)). Quantification based on the intensity of the pyridyl α-H resonance at $\delta = 9.1$ ppm showed that the Fe(II) species represents about 70% of the original concentration of **2**. Taken together, the EPR and NMR results demonstrate that the expected $Fe^{II}Fe^{III}$ byproduct must dissociate into its mononuclear components in MeCN,
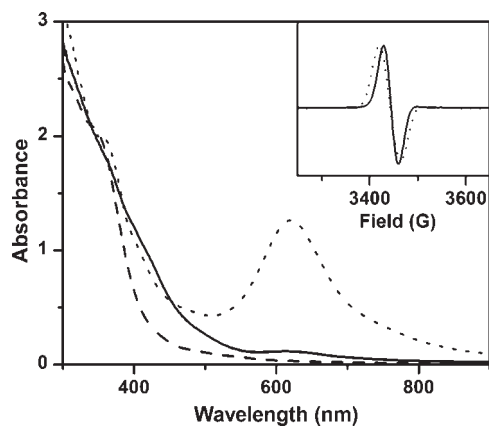
Figure 8. UV–vis spectra of **2** (gray dotted line), **2**−OCH$_3$ resulting from addition of 5 equiv of Bu$_4$NOCH$_3$ (black solid line), and the decay product (black dashed line). Conditions: 3:1 CH$_2$Cl$_2$–MeCN at −80 °C under Ar. Inset: EPR spectra of **2**−OCD$_3$ generated from reaction of **2** with Bu$_4$NOCD$_3$. The solid and dotted traces are of samples with natural abundance Fe and 95% ^{57}Fe, respectively.

Figure 9. The time traces for **2**−OCH$_3$ without any added substrate (bold solid line), in the presence of 2 mM (dashed line) or 10 mM (dotted line) Ph$_3$CH at −80 °C. Inset: The Eyring plot for decay of **2**−OCH$_3$ from −85 to −50 °C (see Table S4 for a list of observed k_{obs} values and Figure S6 for an example of the time-resolved spectral changes observed at −50 °C as well as the time trace at 420 nm together with its fit to a first-order kinetic model). Conditions: in 3:1 CH$_2$Cl$_2$–MeCN under Ar.

similar to what has been reported for $[(\alpha\text{-BPMCN})_2\text{Fe}^{II}\text{Fe}^{III}\text{-}(\mu\text{-OH})_2]^{3+}$ (BPMCN = N,N'-dimethyl-N,N'-bis(2-pyridylmethyl)-*trans*-1,2-diaminocyclohexane).[51] The somewhat higher concentration of Fe(III) as compared to Fe(II) very likely results from partial oxidation of the latter by residual **2** in the course of the reaction.

The ability of **1** and **2** to serve as a 2-e$^-$ oxidant in methanol oxidation may be a consequence of the intramolecular character of this reaction, which allows tight coupling of the two one-electron oxidation steps associated with the oxidation of methanol to formaldehyde. In contrast, for the intermolecular oxidation of hydrocarbons, the nascent alkyl radical formed in the first step can easily diffuse away and be oxidized by a second molecule of **1** or **2**.

In sharp contrast to the observed behavior of **1** and **2**, the $[\text{Fe}^{IV}_2(\mu\text{-O})_2]$ complex **4** (the 1-e$^-$ oxidized derivative of **2**, see Scheme 1) does not exhibit enhanced oxidation ability for methanol. The oxidation of methanol by **4** is in fact very slow; the k_{obs} value for the oxidation of 2 M methanol by **4** is 5 × 10^{-6} s^{-1} at −30 °C (based on the initial decay rate as the reaction was too slow), as compared to a k_{obs} value for **2** is 3.3 × 10^{-5} s^{-1} under the same reaction conditions (Table S3). This comparison indicates that **2** is ∼6-fold more reactive than **4**, despite the fact that **2** is 1-e$^-$ reduced relative to **4**. On the other hand, **4** oxidizes DHA 10-fold faster than **2** in dry MeCN.[36] We attribute the sluggish behavior of **4** to its more stable diamond core structure that strongly favors the left side of the equilibrium shown in Scheme 3. This interpretation is supported by two observations. First, EXAFS analysis shows that the average Fe−O bond distance in **4** is 0.06 Å shorter than that of **2** (1.77 versus 1.83 Å),[36] as more oxidized **4** would be expected to have stronger Fe−O bonds. Second, the exchange of ^{18}O-labeled water into **4** is significantly slower than for **2**;[35,52] complete exchange is achieved in 3 h for **4** at −30 °C versus less than 10 min for **2** (see Figure 7 of the Supporting Information of ref 36). Label exchange with H$_2$^{18}O would require the $[\text{Fe}_2(\mu\text{-O})_2]$ core to open upon attack of the water nucleophile in an equilibrium like that shown in Scheme 3, followed by oxygen−atom interchange. The observed differences between **2** and **4** thus support the
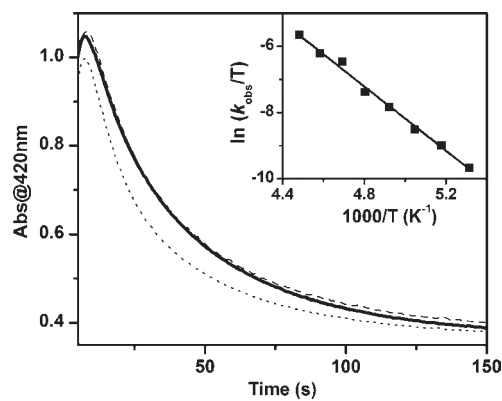
notion that $[\text{Fe}_2(\mu\text{-O})_2]$ core opening is critical for facile C−H bond cleavage by **1** and **2**.

Formation and Properties of the Methoxide Adduct. As a test of the mechanistic hypothesis presented in Scheme 3, we treated **2** with methoxide to trap and characterize the putative **2**−methoxide adduct. Addition of 5 equiv of tetrabutylammonium methoxide (Bu$_4$NOCH$_3$)[53] to **2** at −80 °C causes rapid decay of its characteristic 620 nm chromophore and formation of a new species with a UV−vis absorption spectrum that resembles **2**−OH (Figure 8).[37] The EPR spectrum of this solution shows an isotropic $S = 1/2$ signal with $g = 2.00$ and exhibits ^{57}Fe hyperfine broadening (Figure 8, inset), properties like those of **2**−OH.[37,54] The striking spectroscopic similarity strongly suggests that coordination of methoxide to **2** generates a complex with a $[\text{CH}_3\text{O}−\text{Fe}^{III}−\text{O}−\text{Fe}^{IV}=\text{O}]$ core structure (**2**−OCH$_3$). The spectroscopic similarities also suggest that the terminal oxoiron(IV) moiety of **2**−OCH$_3$ is high-spin ($S = 2$), which should be a potent oxidant for C−H bond cleavage.[37] Double integration of the $S = 1/2$ signal shows that the methoxide adduct can be generated in about 70% yield with respect to **2**. In this experiment, the adduct was generated with Bu$_4$NOCD$_3$ to lengthen the lifetime of **2**−methoxide. However, even **2**−OCD$_3$ decayed quite quickly at −80 °C ($t_{1/2} \approx 200$ s versus 40 s for **2**−OCH$_3$). Partial decay of the **2**−OCD$_3$ sample in the course of EPR sample preparation might result in the underestimation of its yield.

The 400 nm chromophore of **2**−OCH$_3$ decays with a first-order rate constant (k_{obs}) of 0.024 s^{-1} (Figure 9), and methoxide is oxidized to formaldehyde in 30% yield with respect to **2**. Changing the concentration of Bu$_4$NOCH$_3$ from 5 to 20 equiv gives rise to the same k_{obs} within experimental error. The lack of a substrate-concentration dependence in the decay of the chromophore strongly suggests that it is an intramolecular reaction in which the coordinated methoxide group is oxidized. The decay rate of **2**−OCH$_3$ is slowed by a factor of 5 when Bu$_4$NOCD$_3$ is used, showing that H-atom abstraction is a key component of the rate-determining step. However, less formaldehyde (10% versus 30%) is formed in this case. This observation suggests the involvement of competing decay pathways such as ligand

16662

dx.doi.org/10.1021/ja207131g |*J. Am. Chem. Soc.* 2011, 133, 16657–16667

oxidation, and the actual KIE for the oxidation of methoxide is likely to be greater than 5.

The 30% yield of formaldehyde from the self-decay of $2-OCH_3$ at $-80\ ^\circ C$ is much lower than the 90% yield obtained from the reaction of **2** with methanol at $-30\ ^\circ C$. For the latter, **2** acts as a 2-e^- oxidant and is reduced to an $Fe^{II}Fe^{III}$ product. In contrast, the solution of the decayed $2-OCH_3$ is EPR silent and shows the characteristic $\sim$350 nm absorption feature (Figure 8, dashed line) of an $Fe^{III}-O-Fe^{III}$ species (see Figure 3 for the UV–vis spectrum of such a complex). $2-OCH_3$ would thus appear to act as a 1-e^- oxidant at $-80\ ^\circ C$. The different outcomes probably stem from the higher concentration of available reactive species in the $2-OCH_3$ solution and the slower rate of substrate oxidation at lower temperature, both of which would allow the initial $Fe^{II}Fe^{III}$ product that is formed in the 2-e^- oxidation of methoxide to be rapidly oxidized to the $Fe^{III}Fe^{III}$ complex by residual $2-OCH_3$.

On the basis of the solid green line plotted in Figure 2, the strong C–H bond of methanol ($D_{C-H} = 96$ kcal mol^{-1}) should be cleaved by **1** more slowly by 4–5 orders of magnitude than the much weaker C–H bonds of triphenylmethane (Ph$_3$C–H, $D_{C-H} = 81$ kcal mol^{-1}) and DHA ($D_{C-H} = 78$ kcal mol^{-1}). However, upon coordination of the methoxide group to **2** to generate $2-OCH_3$, the intramolecular oxidation of the methyl group can become competitive with the intermolecular oxidation of added substrates, depending on the concentration of the added substrate. As shown in Figure 9, the decay rate of $2-OCH_3$ at $-80\ ^\circ C$ is not changed when 2 mM Ph$_3$CH is added, and the yield of formaldehyde (28%) is nearly identical to that without Ph$_3$CH. When 10 mM Ph$_3$CH is added, the decay rate of $2-OCH_3$ becomes noticeably faster and the formaldehyde yield decreases to 16%. Concomitantly, a 6% yield of Ph$_3$COH from Ph$_3$CH oxidation can be detected. Competitive oxidations of CH$_3$OH and hydrocarbon substrates by **2** at $-30\ ^\circ C$ also lead to the same conclusion. For example, addition of 2 mM Ph$_3$CH to the mixture of **2** and 1 M methanol in MeCN at $-30\ ^\circ C$ changes neither the reaction rate nor the yield of formaldehyde. When 10 mM DHA is added to the mixture of **2** and 1 M methanol, the yield of formaldehyde decreases from 90% to 44%, and 20% anthracene can be detected. These results confirm that methanol can compete with hydrocarbon substrates with significantly weaker C–H bonds by coordination to the iron center to elicit an intramolecular oxidation pathway.

The inset of Figure 9 shows the Eyring plot for the decay of $2-OCH_3$ in the temperature range of -85 to $-50\ ^\circ C$. The activation parameters calculated from the plot are $\Delta H^{\ddagger} = 9.7(2)$ kcal mol^{-1} and $\Delta S^{\ddagger} = -15(2)$ cal mol^{-1} K^{-1}. For comparison, $\Delta H^{\ddagger}$ and $\Delta S^{\ddagger}$ values of 15.6 kcal mol^{-1} and -14 cal mol^{-1} K^{-1}, respectively, are reported for the self-decay of $[Fe^{IV}(O)-(TMG_3tren)]^{2+}$ (TMG$_3$tren = 1,1,1-tris{2-[N^2-(1,1,3,3-tetramethyl-guanidino)]-ethyl}amine), another complex with an $S = 2$ $Fe^{IV}=O$ unit. Self-decay of $[Fe^{IV}(O)(TMG_3tren)]^{2+}$ occurs via intramolecular attack of a ligand methyl group.[55] The two reactions have similarly small $\Delta S^{\ddagger}$ values, which are consistent with an intramolecular oxidation mechanism. Notably, the self-decay of $2-OCH_3$ has a lower activation enthalpy by 6 kcal mol^{-1}, a gap that would widen further when the difference in bond dissociation energy between NCH$_2$–H and OCH$_2$–H bonds is taken into account. As an illustration, we note that the lifetimes of the two complexes are comparable but at temperatures that differ by 105 $^\circ C$ ($t_{1/2} = 40$ s at $-80\ ^\circ C$ for $2-OCH_3$ versus 30 s at 25 $^\circ C$ for $[Fe^{IV}(O)(TMG_3tren)]^{2+}$).[55] Thus, the
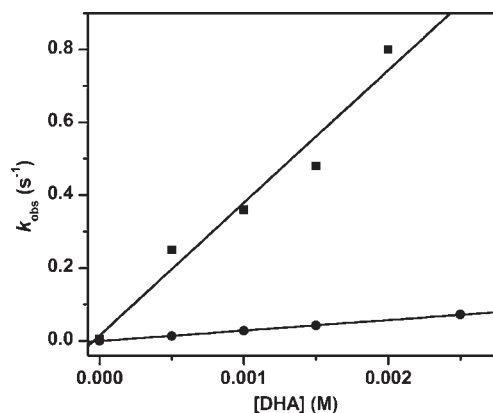
Figure 10. k_{obs} versus [DHA] plot for oxidation of DHA by $2-OCD_3$ (■) and $2-OH$ (●) in 3:1 CH$_2$Cl$_2$–MeCN at $-80\ ^\circ C$ under Ar. See Figure S7 for an example of the time-resolved spectral changes during DHA oxidation by $2-OCD_3$ as well as the time trace at 420 nm together with its fit to a first-order kinetic model.

$Fe^{IV}=O$ unit in $2-OCH_3$ is a significantly more reactive C–H bond cleaving agent than $[Fe^{IV}(O)(TMG_3tren)]^{2+}$.

The higher C–H bond cleavage reactivity of $2-OCH_3$ can also be illustrated by its intermolecular oxidation of DHA. At $-80\ ^\circ C$ in 3:1 CH$_2$Cl$_2$–CH$_3$CN, $2-OCH_3$ oxidizes DHA with a second-order rate constant of 360 M^{-1} s^{-1} (Figure 10). (To slow self-decay and obtain a higher yield of **2**–methoxide prior to DHA addition, $2-OCD_3$ was used to measure the data presented in Figure 10. However, the DHA oxidation rates by $2-OCH_3$ and $2-OCD_3$ are identical.) Under the same conditions, **2** and $2-OH$, respectively, have k_2 values of 10^{-5} and 28 M^{-1} s^{-1}.[37] Thus, $2-OCH_3$ is 13-fold even more reactive than $2-OH$ and 3.6×10^7 more oxidizing than its precursor **2**. The large difference in rates between **2** and $2-OH$ has been attributed to the core isomerization shown in Scheme 2 converting a bridging oxo to a terminal oxo moiety with a concomitant change of the iron(IV) spin state from $S = 1$ to $S = 2$.[37] According to a thermochemical cycle developed by Bordwell[56] and applied by Mayer to metal–oxo systems,[57,58] the H-atom abstraction (HAA) reactivity, which is equivalent to O–H BDE value, is a function of the one-electron reduction potential of the M = O oxidant and the pK_a of the M–OH reduction product.[58,59] After HAA, the $[Fe-O-Fe^{IV}=O]$ motif in ring-opened structures is reduced to $[Fe-O-Fe^{III}-OH]$. We would argue that this reduced form should have a significantly higher pK_a than the reduced $[Fe-OH-Fe^{III}]$ form of a diamond core and contribute to the much higher HAA reactivity of ring-opened structures.[36,37]

Despite the fact that $2-OH$ and $2-OCH_3$ share the same $X-Fe^{III}-O-Fe^{IV}=O$ core, the latter is still a 13-fold more powerful oxidant. One might attribute this increased reactivity to the higher basicity of the methoxide ligand, which could in turn increase the pK_a of the $[X-Fe^{III}-O-Fe^{III}-OH]$ product resulting from HAA. However, as methoxide and hydroxide differ by only one pK_a unit,[49] the X ligand might not be able to exert a significant effect on the pK_a of the $Fe^{III}-OH$ that is four bonds away. In our opinion, a much more likely rationale is the presence of a hydrogen-bonding interaction between the bound hydroxide and the Fe$=$O unit of $2-OH$, evidence for which has been obtained for its one-electron oxidized diiron(IV) analog.[50] On the basis of a comparison of the reactivities of two iron(IV)

Scheme 4. Core Structures and Spin States of the Iron(IV) Centers of a Series of Diiron Complexes Supported by a Common Tetradentate Ligand, Together with Their Relative Rates of DHA Oxidation in 3:1 CH$_2$Cl$_2$–MeCN at −80 °C^a

Complex	2	4	5	2-OH	2-OCH$_3$
Spin state of Fe^{IV}	S = 1	S = 1	S = 1	S = 2	S = 2
Relative reactivity	1	10	2.7 x 10^3	2.8 x 10^6	3.6 x 10^7

^{a} Data for the relative reactivities of complexes **2**, **4**, **5**, and **2**−OH were taken from ref 37.

complexes supported by the same tetradentate ligand but with an oxo unit in one and a hydroxo ligand in the other,[60] the presence of this H-bond in **2**−OH and its absence of **2**−OCH$_3$ would be expected to result in the attenuation of the H-atom abstracting capability of **2**−OH. In striking contrast, the core isomerization associated with **2** does not appear to occur with **4**, its one-electron oxidized derivative, probably due to its more robust core structure.

The C−H bond cleavage reactivity of **2**−OCH$_3$ can be compared to that of the most reactive mononuclear S = 2 oxoiron(IV) complex reported to date. [Fe^{IV}(O)(OH$_2$)$_5$]$^{2+}$ is generated from the reaction of Fe^{2+} in acidic aqueous solution with O$_3$.[61,62] A second-order rate constant of 572 M^{-1} s^{-1} has been determined for the reaction of the latter complex with methanol in aqueous solution at 25 °C.[61] A pseudofirst-order rate constant of 572 s^{-1} can thus be calculated for its reaction with 1 M methanol and compared to the value of 260 s^{-1} for the self-decay of **2**−OCH$_3$ at 25 °C, which is estimated from an extrapolation of the Eyring plot in Figure 9. Thus, these two complexes would appear to be comparable in H-atom abstracting ability. The corresponding **1**−OCH$_3$ adduct should be even more oxidizing, as suggested by the 12-fold higher oxidation rate of methanol by **1** at −30 °C as compared to that for **2** (see Table S3).

Lastly, we highlight a recently reported mononuclear S = 1 oxoiron(IV) complex supported by the tris((N-methylbenzimi-dazol-2-yl)methyl)amine ligand, which was found to be comparably reactive to **2**−OH.[63] This complex is much more reactive than the other S = 1 oxoiron(IV) complexes reported thus far,[41−44,64] due to a closely lying and easily accessible S = 2 state.[63] These results show that making direct comparisons of reactivity among complexes with different supporting ligands is difficult, and more complexes need to be synthesized to augment the current collection of oxoiron(IV) complexes and refine our understanding of how spin state affects C−H bond cleavage reactivity.

■ SUMMARY AND PERSPECTIVES

In this study, we have demonstrated that [Fe^{III}Fe^{IV}(μ-O)$_2$] complexes **1** and **2**, which are sluggish in the oxidation of C−H bonds, can be activated by water or methanol to generate a much more reactive H-atom abstraction agent. This activation is proposed to result from the binding of hydroxide or methoxide to the [Fe^{III}Fe^{IV}(μ-O)$_2$] core, forming an open-core [X−Fe^{III}−O−Fe^{IV}=O] adduct (Scheme 3). The putative methoxide adduct has been trapped at −80 °C by treatment of **2** with 5 equiv of methoxide, the adduct lifetime having been extended by the presence of three electron-donating substituents on all three pyridine donors of the supporting ligand and the deuteration of its benzylic hydrogens. Thus, **2**−OCH$_3$ belongs to a unique

series of high-valent diiron complexes supported by the same tetradentate ligand (L^2 in Scheme 1) that exhibit dramatically different C−H bond cleavage rates.

Scheme 4 illustrates the core structures of this series of high-valent diiron complexes and compares their relative abilities to cleave C−H bonds. The 7 order-of-magnitude jump in the DHA oxidation rate on going from **2** to **2**−OCH$_3$ emphasizes that the core structure and the spin state of the Fe^{IV}=O unit significantly influence the reactivities of the high-valent diiron intermediates. The fact that high-spin complexes **2**−OCH$_3$ and **2**−OH are much more reactive than the corresponding diiron(IV) complex with a S = 1 Fe^{IV}=O moiety (**5** in Scheme 4) provides strong experimental support for the prediction from several independent DFT calculations for a much higher reactivity of an S = 2 Fe^{IV}=O unit relative to an S = 1 Fe^{IV}=O unit.[65−68] The comparison made in Scheme 4 strongly suggests that the higher H-atom abstraction reactivity of **2**−OCH$_3$ is a consequence of two factors: (a) the transformation of the bridging oxo of **2** to a terminal oxo unit in **2**−OCH$_3$ and (b) the conversion of an S = 1 Fe^{IV}=O unit to an S = 2 Fe^{IV}=O unit. The fact that these complexes share a common oxoiron(IV)−tetradentate ligand unit makes this conclusion particularly persuasive.

Moreover, **2**−OCH$_3$ represents a rare example of a spectro-scopically characterized adduct of a high-valent oxidant and a substrate, with the oxidation of the latter being significantly facilitated by an intramolecular mechanism. Indeed, such an intramolecular strategy has been used to demonstrate the activation of dioxygen or peroxides by a number of biomimetic nonheme iron complexes, resulting in the regiospecific oxidation of a pendant group on the supporting ligand,[69−81] but the presumed high-valent iron−oxo oxidant has not been stable enough to be observed. What makes the chemistry of the diiron complexes **1** and **2** particularly unique is the possibility for substrate-induced activation of the Fe$_2$O$_2$ diamond core, where substrate binding to one iron unmasks a highly reactive adjacent S = 2 Fe^{IV}=O for attack of the substrate C−H bond. A similar core isomerization mechanism could also be employed by intermediate **Q** of soluble methane monooxygenase (sMMO-**Q**) for its highly selective oxidation of methane. Core isomerization to the hyper-reactive ring-opened form would occur only when substrate is present as a strategy to protect the weaker C−H bonds present in the amino acid residues that line the diiron active site of sMMO. Although DFT calculations to date support the notion of methane attack by the intact [Fe^{IV}$_2$(μ-O)$_2$] core of sMMO-**Q**,[14,25,30,31] kinetic studies of the reactions of sMMO-**Q** with alkanes are not incompatible with the core isomerization idea. Brazeau and Lipscomb have demonstrated a two-step mechanism involving substrate binding to form a **Q·S** adduct followed by adduct decomposition via C−H bond cleavage, with the latter being rate determining only in the case of methane.[11,12] Core isomerization could occur either upon adduct formation or in the subsequent transition state leading to substrate oxidation, representing a unique mechanistic feature available only for diiron enzymes. Spectroscopic characterization of the thus far elusive **Q·S** adduct should provide a test of the core isomerization hypothesis and greatly improve our understanding of the catalytic mechanism of sMMO.

■ EXPERIMENTAL SECTION

Physical Methods. UV−vis spectra and kinetic time traces were recorded on a Hewlett-Packard 8453A diode array spectrometer equipped

with a cryostat from Unisoku Scientific Instruments, Osaka, Japan. This combination allows kinetic studies to be performed at temperatures down to −85 °C and to record a spectrum every 0.1 s. For some rapid reactions with a reaction time of 10 s, time traces at one wavelength can be obtained with about 100 data points for reliable kinetic fits (see Figures S6 and S7). Perpendicular mode X-band (9.63 GHz) EPR spectra were recorded on a Bruker Elexsys E500 spectrometer equipped with an Oxford Instrument ESR-10 liquid helium cryostat. The quantification of all signals was relative to a Cu(II)-EDTA spin standard. NMR data were collected on a Varian VI-500 spectrometer. Gas chromatograms were measured on a PerkinElmer Autosystem XL equipped with a polar column.

Materials. 9,10-Dihydroanthracene (DHA, 97%) purchased from Aldrich was recrystallized twice from EtOH under Ar. 9,9,10,10-d_4-DHA was synthesized according to reported procedures.[37] 1,2,3,4-Tetrahydronaphthalene (tetralin, 99%) purchased from Aldrich was passed through neutral Al_2O_3. All deuterated solvents were purchased from Cambridge Isotope Laboratories and dried over molecular sieves (3A). Anhydrous dichloromethane (>99.8%) and MeCN (>99.8%), xanthene (99%), fluorene (>99%), triphenylmethane (99%), ethylbenzene (99.8%), toluene (99.8%), benzyl alcohol (99.8%), 1-hexanol (>99%), 2-hexanol (99%), isobutanol (>99%), ethanol (>99.5%), methanol (99.8%), diphenylmethanol (99%), tetrabutylammonium methoxide (Bu_4NOCH_3) (20% in methanol), and all other chemicals were purchased from Aldrich and used as received. To prepare Bu_4-$NOCD_3$, the methanol solvent for a 1 mL solution of Bu_4NOCH_3 was removed under vacuum, and 1 mL of CD_3OD (dried over activated neutral Al_2O_3) was added to the resulting oily product to exchange with CH_3O^- for 30 min. This procedure was repeated three times. NMR of the final solution in CD_3OD confirmed that that the product was completely deuterated.

Complexes **1**, **2**, and **4** were synthesized according to reported procedures.[35−37] The solid products were dissolved in desired solvents to about 0.2 mM for kinetic studies and 0.5 mM for product-yield analysis or preparation of **2**−methoxide EPR samples. Solutions of **3** (~2.0 mM) were generated from reaction of the $[LFe^{II}(MeCN)_2]$-$(OTf)_2$ with 1 equiv of peracetic acid in MeCN at −40 °C.[46]

General Procedures for Kinetic Studies and Product Analysis. An appropriate amount of substrate (in CH_2Cl_2 stock solution) was added to the stirred complex solution maintained at −30 °C in a 1 cm cuvette, and the decay time trace of the chromophore at 616 nm (for **1**), 620 nm (**2**), 720 nm (for **3**), or 875 nm (for **4**) was then monitored. Time traces were subjected to a pseudofirst-order fit, and second-order rate constants were obtained from concentration dependence data. The methoxide adduct (**2**−methoxide) was generated by adding 5 equiv of Bu_4NOCH_3 or Bu_4NOCD_3 to **2** in a 3:1 CH_2Cl_2−MeCN mixture. The decay of **2**−methoxide was monitored by the absorption at 420 nm.

Typically, the yields of oxidation products were quantified by GC, with naphthalene as the internal standard. The anthracene product was quantified by its UV−vis absorption at 377 nm (ε = 7700 M^{-1} cm^{-1}) obtained after removing iron complexes from the reaction solutions by silica gel columns. Formaldehyde from methanol/methoxide oxidation was quantified by following a reported colorimetric procedure.[82] The assay solution contained 0.4 M ammonium acetate, 0.02 M acetic acid, 0.02 M acetylacetone, and 0.001 M Na_2EDTA (for decomposing iron complexes) in H_2O. The calibration curve was obtained by mixing 1.5 mL of assay solution with 0.5 mL of MeCN solution containing 0.1−0.5 mM added formaldehyde standard and 0.5 mM diiron(III) complex (precursor of **2**). For a typical assay experiment, 1.5 mL of assay solution and 0.5 mL of reaction solution were mixed, stirred at room temperature for 16 h, and then subjected to measurement of the 412 nm absorption. If CH_2Cl_2 was present in the reaction solution (for methoxide oxidation), it was removed carefully with a rotary evaporator after 16 h of

stirring, and the assay solution was added to the remaining solution to reach a total volume of 2.0 mL prior to UV−vis measurement.

■ ASSOCIATED CONTENT

Ⓢ **Supporting Information.** Figures S1, S2, S6, and S7 showing examples of time-resolved spectral changes and corresponding single-wavelength time traces together with fits to a first-order kinetic model, Figures S4 and S5 showing the kinetics of DHA oxidation by **1**, and tables listing the rate constants associated with Figures 2, 6, 9, and S2. This material is available free of charge via the Internet at http://pubs.acs.org.

■ AUTHOR INFORMATION

Corresponding Author
larryque@umn.edu

Present Address
†Department of Physical Chemistry of Fuel Fossils, Institute of Physical Organic Chemistry and Chemistry of Coal, NAS of Ukraine, Lviv, Ukraine.

■ REFERENCES

(1) Wallar, B. J.; Lipscomb, J. D. *Chem. Rev.* **1996**, *96*, 2625–2658.

(2) Kurtz, D. M., Jr. *J. Biol. Inorg. Chem.* **1997**, *2*, 159–167.

(3) Solomon, E. I.; Brunold, T. C.; Davis, M. I.; Kemsley, J. N.; Lee, S.-K.; Lehnert, N.; Neese, F.; Skulan, A. J.; Yang, Y.-S.; Zhou, J. *Chem. Rev.* **2000**, *100*, 235–349.

(4) Fox, B. G.; Lyle, K. S.; Rogge, C. E. *Acc. Chem. Res.* **2004**, *37*, 421–429.

(5) Murray, L. J.; Lippard, S. J. *Acc. Chem. Res.* **2007**, *40*, 466–474.

(6) Tinberg, C. E.; Lippard, S. J. *Acc. Chem. Res.* **2011**, *44*, 280–288.

(7) Groves, J. T. *J. Inorg. Biochem.* **2006**, *100*, 434–447.

(8) Lee, S.-K.; Fox, B. G.; Froland, W. A.; Lipscomb, J. D.; Münck, E. *J. Am. Chem. Soc.* **1993**, *115*, 6450–6451.

(9) Lee, S.-K.; Nesheim, J. C.; Lipscomb, J. D. *J. Biol. Chem.* **1993**, *268*, 21569–21577.

(10) Liu, K. E.; Valentine, A. M.; Wang, D.; Huynh, B. H.; Edmondson, D. E.; Salifoglou, A.; Lippard, S. J. *J. Am. Chem. Soc.* **1995**, *117*, 10174–10185.

(11) Brazeau, B. J.; Lipscomb, J. D. *Biochemistry* **2000**, *39*, 13503–13515.

(12) Brazeau, B. J.; Wallar, B. J.; Lipscomb, J. D. *J. Am. Chem. Soc.* **2001**, *123*, 10421–10422.

(13) Brazeau, B. J.; Austin, R. N.; Tarr, C.; Groves, J. T.; Lipscomb, J. D. *J. Am. Chem. Soc.* **2001**, *123*, 11831–11837.

(14) Baik, M.-H.; Newcomb, M.; Friesner, R. A.; Lippard, S. J. *Chem. Rev.* **2003**, *103*, 2385–2420.

(15) Shu, L.; Nesheim, J. C.; Kauffmann, K.; Münck, E.; Lipscomb, J. D.; Que, L., Jr. *Science* **1997**, *275*, 515–518.

(16) Broadwater, J. A.; Ai, J.; Loehr, T. M.; Sanders-Loehr, J.; Fox, B. G. *Biochemistry* **1998**, *37*, 14664–14671.

(17) Murray, L. J.; Naik, S. G.; Ortillo, D. O.; García-Serres, R.; Lee, J. K.; Huynh, B. H.; Lippard, S. J. *J. Am. Chem. Soc.* **2007**, *129*, 14500–14510.

(18) Vu, V. V.; Emerson, J. P.; Martinho, M.; Kim, Y. S.; Münck, E.; Park, M. H.; Que, L., Jr. *Proc. Natl. Acad. Sci. U.S.A.* **2009**, *106*, 14814–14819.

16665

dx.doi.org/10.1021/ja207131g |*J. Am. Chem. Soc.* 2011, 133, 16657–16667

(19) Nordlund, P.; Reichard, P. *Annu. Rev. Biochem.* **2006**, *75*, 681–706.

(20) Bollinger, J. M., Jr.; Krebs, C. *J. Inorg. Biochem.* **2006**, *100*, 586–605.

(21) Bollinger, J. M., Jr.; Jiang, W.; Green, M. T.; Krebs, C. *Curr. Opin. Struct. Biol.* **2008**, *18*, 650–657.

(22) Younker, J. M.; Krest, C. M.; Jiang, W.; Krebs, C.; Bollinger, J. M., Jr.; Green, M. T. *J. Am. Chem. Soc.* **2008**, *130*, 15022–15027.

(23) Ambundo, E. A.; Friesner, R. A.; Lippard, S. J. *J. Am. Chem. Soc.* **2002**, *124*, 8770–8771.

(24) Luo, Y.-R. *Comprehensive Handbook of Chemical Bond Energies*; CRC Press: Boca Raton, FL, 2007.

(25) Gherman, B. F.; Lippard, S. J.; Friesner, R. A. *J. Am. Chem. Soc.* **2005**, *127*, 1025–1037.

(26) Wallar, B. J.; Lipscomb, J. D. *Biochemistry* **2001**, *40*, 2220–2233.

(27) Brazeau, B. J.; Lipscomb, J. D. *Biochemistry* **2003**, *42*, 5618–5631.

(28) Rauk, A.; Yu, D.; Taylor, J.; Shustov, G. V.; Block, D. A.; Armstrong, D. A. *Biochemistry* **1999**, *38*, 9089–9096.

(29) Tinberg, C. E.; Lippard, S. J. *Biochemistry* **2009**, *48*, 12145–12158.

(30) Siegbahn, P. E. M.; Crabtree, R. H. *J. Am. Chem. Soc.* **1997**, *119*, 3103–3113.

(31) Rinaldo, D.; Philipp, D. M.; Lippard, S. J.; Friesner, R. A. *J. Am. Chem. Soc.* **2007**, *129*, 3135–3147.

(32) Foster, T. L.; Caradonna, J. P. *J. Am. Chem. Soc.* **2003**, *125*, 3678–3679.

(33) Rowe, G. T.; Rybak-Akimova, E. V.; Caradonna, J. P. *Inorg. Chem.* **2007**, *46*, 10594–10606.

(34) Rowe, G. T.; Rybak-Akimova, E. V.; Caradonna, J. P. *Chem.-Eur. J.* **2008**, *14*, 8303–8311.

(35) Dong, Y.; Fujii, H.; Hendrich, M. P.; Leising, R. A.; Pan, G.; Randall, C. R.; Wilkinson, E. C.; Zang, Y.; Que, L., Jr.; Fox, B. G.; Kauffmann, K.; Münck, E. *J. Am. Chem. Soc.* **1995**, *117*, 2778–2792.

(36) Xue, G.; Wang, D.; De Hont, R.; Fiedler, A. T.; Shan, X.; Münck, E.; Que, L., Jr. *Proc. Natl. Acad. Sci. U.S.A.* **2007**, *104*, 20713–20718.

(37) Xue, G.; De Hont, R.; Münck, E.; Que, L., Jr. *Nat. Chem.* **2010**, *2*, 400–405.

(38) Johansson, A. J.; Noack, H.; Siegbahn, P. E. M.; Xue, G.; Que, L., Jr. *Dalton Trans.* **2009**, 6741–6750.

(39) Klinker, E. J.; Shaik, S.; Hirao, H.; Que, L., Jr. *Angew. Chem., Int. Ed.* **2009**, *48*, 1291–1295.

(40) It is possible that there are trace amounts of water from commercial available anhydrous MeCN (specified as containing <0.001% (5×10^{-4} M)) and from complex **1**, which was dried under vacuum at 0 °C for less than 10 min.

(41) Kaizer, J.; Klinker, E. J.; Oh, N. Y.; Rohde, J.-U.; Song, W. J.; Stubna, A.; Kim, J.; Münck, E.; Nam, W.; Que, L., Jr. *J. Am. Chem. Soc.* **2004**, *126*, 472–473.

(42) Sastri, C. V.; Lee, J.; Oh, K.; Y.J., L.; Lee, J.; Jackson, T. A.; Ray, K.; Hirao, H.; Shin, W.; Halfen, J. A.; Kim, J.; Que, L., Jr.; Shaik, S.; Nam, W. *Proc. Natl. Acad. Sci. U.S.A.* **2007**, *104*, 19181–19186.

(43) Yoon, J.; Wilson, S. A.; Jang, Y. K.; Seo, M. S.; Nehru, K.; Hedman, B.; Hodgson, K. O.; Bill, E.; Solomon, E. I.; Nam, W. *Angew. Chem., Int. Ed.* **2009**, *48*, 1257–1260.

(44) Company, A.; Prat, I.; Frisch, J. R.; Mas-Ballesté, R.; Güell, M.; Juhász, G.; Ribas, X.; Münck, E.; Luis, J. M.; Que, L., Jr.; Costas, M. *Chem.-Eur. J.* **2011**, *17*, 1622–1634.

(45) Goldsmith, C. R.; Jonas, R. T.; Stack, T. D. P. *J. Am. Chem. Soc.* **2002**, *124*, 83–96.

(46) Lim, M. H.; Rohde, J.-U.; Stubna, A.; Bukowski, M. R.; Costas, M.; Ho, R. Y. N.; Münck, E.; Nam, W.; Que, L., Jr. *Proc. Natl. Acad. Sci. U.S.A.* **2003**, *100*, 3665–3670.

(47) Clarke, K.; Rothwell, K. *J. Chem. Soc.* **1960**, 1885–1895.

(48) Our detailed studies of **2**−OCH$_3$ suggest that the amount of **1**−OR formed in the reaction of **1** with alcohols at −30 °C represents only a very minor fraction of the species in solution. This inference is

(49) *CRC Handbook of Chemistry and Physics*, 77th ed.; Lide, D. R., Ed.; CRC Press, Inc.: New York, 1996.

(50) Xue, G.; Fiedler, A. T.; Martinho, M.; Münck, E.; Que, L., Jr. *Proc. Natl. Acad. Sci. U.S.A.* **2008**, *105*, 20615–20620.

(51) Stubna, A.; Jo, D.-H.; Costas, M.; Brenessel, W. W.; Andres, H.; Bominaar, E. L.; Münck, E.; Que, L., Jr. *Inorg. Chem.* **2004**, *43*, 3067–3079.

(52) Wilkinson, E. C.; Dong, Y.; Zang, Y.; Fujii, H.; Fraczkiewicz, R.; Fraczkiewicz, G.; Czernuszewicz, R. S.; Que, L., Jr. *J. Am. Chem. Soc.* **1998**, *120*, 955–962.

(53) The very short lifetime of **2**−OCH$_3$, even at −80 °C, prevented us from performing titration experiments to determine how much Bu$_4$NOCH$_3$ was required for complete conversion of **2** to **2**−OCH$_3$ and estimate the binding constant for the methoxide.

(54) De Hont, R. F.; Xue, G.; Hendrich, M. P.; Que, L., Jr.; Bominaar, E. L.; Münck, E. *Inorg. Chem.* **2010**, *49*, 8310–8322.

(55) England, J.; Guo, Y.; Farquhar, E. R.; Young, V. G., Jr.; Münck, E.; Que, L., Jr. *J. Am. Chem. Soc.* **2010**, *132*, 8635–8644.

(56) Bordwell, F. G.; Cheng, J.-P.; Ji, G.-Z.; Satish, A. V.; Zhang, X. *J. Am. Chem. Soc.* **1991**, *113*, 9790–9795.

(57) Gardner, K. A.; Mayer, J. M. *Science* **1995**, *269*, 1849–1851.

(58) Warren, J. J.; Tronic, T. A.; Mayer, J. M. *Chem. Rev.* **2010**, *110*, 6961–7001.

(59) Mayer, J. M. *Acc. Chem. Res.* **1998**, *31*, 441–450.

(60) Fiedler, A. T.; Que, L., Jr. *Inorg. Chem.* **2009**, *48*, 11038–11047.

(61) Pestovsky, O.; Bakac, A. *J. Am. Chem. Soc.* **2004**, *126*, 13757–13764.

(62) Pestovsky, O.; Stoian, S.; Bominaar, E. L.; Shan, X.; Münck, E.; Que, L., Jr.; Bakac, A. *Angew. Chem., Int. Ed.* **2005**, *44*, 6871–6874.

(63) Seo, M. S.; Kim, N. K.; Cho, K.-B.; So, J. E.; Park, S. K.; Clémancey, M.; Garcia-Serres, R.; Latour, J.-M.; Shaik, S.; Nam, W. *Chem. Sci.* **2011**, *2*, 1039–1045.

(64) Hong, S.; Lee, Y.-M.; Cho, K.-B.; Sundaravel, K.; Cho, J.; Kim, M. J.; Shin, W.; Nam, W. *J. Am. Chem. Soc.* **2011**, *133*, 11876–11879.

(65) Kumar, D.; Hirao, H.; Que, L., Jr.; Shaik, S. *J. Am. Chem. Soc.* **2005**, *127*, 8026–8027.

(66) Shaik, S.; Hirao, H.; Kumar, D. *Acc. Chem. Res.* **2007**, *40*, 532–542.

(67) Decker, A.; Rohde, J.-U.; Klinker, E. J.; Wong, S. D.; Que, L., Jr.; Solomon, E. I. *J. Am. Chem. Soc.* **2007**, *129*, 15983–15996.

(68) Ye, S.; Neese, F. *Curr. Opin. Chem. Biol.* **2009**, *13*, 89–98.

(69) Ménage, S.; Galey, J.-B.; Hussler, G.; Seité, M.; Fontecave, M. *Angew. Chem., Int. Ed. Engl.* **1996**, *35*, 2353–5355.

(70) Ménage, S.; Galey, J.-B.; Dumats, J.; Hussler, G.; Seité, M.; Luneau, I. G.; Chottard, G.; Fontecave, M. *J. Am. Chem. Soc.* **1998**, *120*, 13370–13382.

(71) Lange, S. J.; Miyake, H.; Que, L., Jr. *J. Am. Chem. Soc.* **1999**, *121*, 6330–6331.

(72) Mehn, M. P.; Fujisawa, K.; Hegg, E. L.; Que, L., Jr. *J. Am. Chem. Soc.* **2003**, *125*, 7828–7842.

(73) Jensen, M. P.; Mehn, M. P.; Que, L., Jr. *Angew. Chem., Int. Ed.* **2003**, *42*, 4357–4360.

(74) Yoon, S.; Lippard, S. J. *Inorg. Chem.* **2006**, *45*, 5438–5446.

(75) Korendovych, I. V.; Kryatov, S. V.; Rybak-Akimova, E. V. *Acc. Chem. Res.* **2007**, *40*, 510–521.

(76) Yamashita, M.; Furutachi, H.; Tosha, T.; Fujinami, S.; Saito, W.; Maeda, Y.; Takahashi, K.; Tanaka, K.; Kitagawa, T.; Suzuki, M. *J. Am. Chem. Soc.* **2007**, *129*, 2–3.

based on the Eyring plot shown in Figure 9, from which we can extrapolate a value of 5.3 s^{-1} for the self-decay rate constant (k_{sd}) of **2**−OCH$_3$ at −30 °C. A larger k_{sd} value would be expected for **1**−OCH$_3$ as it is even more reactive. However, the 5.3 s^{-1} value estimated for **2**−OCH$_3$ at −30 °C is 300-fold larger than the k_{obs} of 0.014 s^{-1} measured for methanol oxidation by **1** in the presence of 1 M methanol and 10 mM 2,4,6-collidine at the same temperature, suggesting that the putative **1**−OCH$_3$ oxidant represents less than 1% of the concentration of **1**. It is thus not surprising that no obvious spectroscopic changes can be detected upon addition of 1 M methanol and 10 mM 2,4,6-collidine to **1**.

(77) Chen, M. S.; White, M. C. *Science* **2007**, *318*, 783–787.

(78) Makhlynets, O. V.; Das, P.; Taktak, S.; Flook, M.; Mas-Ballesté, R.; Rybak-Akimova, E. V.; Que, L., Jr. *Chem.-Eur. J.* **2009**, *15*, 13171–13180.

(79) Mukherjee, A.; Cranswick, M. A.; Chakrabarti, M.; Paine, T. K.; Fujisawa, K.; Münck, E.; Que, L., Jr. *Inorg. Chem.* **2010**, *49*, 3618–3628.

(80) Cavazza, C.; Bochot, C.; Rousselot-Pailley, P.; Carpentier, P.; Cherrier, M. V.; Martin, L.; Marchi-Delapierre, C.; Fontecilla-Camps, J. C.; Ménage, S. *Nat. Chem.* **2010**, *2*, 1069–1076.

(81) Das, P.; Que, L., Jr. *Inorg. Chem.* **2010**, *49*, 9479–9485.

(82) Nash, T. *Biochem. J.* **1953**, *55*, 416–421.